

# Journal of Materials Chemistry A

Accepted Manuscript



This is an *Accepted Manuscript*, which has been through the Royal Society of Chemistry peer review process and has been accepted for publication.

*Accepted Manuscripts* are published online shortly after acceptance, before technical editing, formatting and proof reading. Using this free service, authors can make their results available to the community, in citable form, before we publish the edited article. We will replace this *Accepted Manuscript* with the edited and formatted *Advance Article* as soon as it is available.

You can find more information about *Accepted Manuscripts* in the [Information for Authors](#).

Please note that technical editing may introduce minor changes to the text and/or graphics, which may alter content. The journal's standard [Terms & Conditions](#) and the [Ethical guidelines](#) still apply. In no event shall the Royal Society of Chemistry be held responsible for any errors or omissions in this *Accepted Manuscript* or any consequences arising from the use of any information it contains.



Journal Name

REVIEW

## Recent Advances in the Development of Sunlight-Driven Hollow Structure Photocatalysts and their Applications

Received 00th January 20xx,  
Accepted 00th January 20xx

DOI: 10.1039/x0xx00000x

[www.rsc.org/](http://www.rsc.org/)

Chinh Chien Nguyen, Nhu Nang Vu, and Trong-On Do\*

The over-exploitation of fossil fuels means that research into alternative sustainable energy sources is crucial for the scientific community. The harvesting of solar energy via photocatalysis is a key approach to developing these alternatives. Furthermore, photocatalytic materials show great promise for degradation of pollutants. However, limitations in incident light utilization and charge separation are major drawbacks that restrict the activity of current artificial photosystems. Construction of hollow nano-sized photocatalysts is emerging as a promising approach to fabricating novel and effective materials, as hollow photocatalysts possess unique properties that may be exploited to overcome these challenges. This review gives a concise overview of the advantages of hollow structures for this purpose, the methodology used to prepare hollow photocatalysts, and the current state-of-the-art in the development of hollow structure photocatalysts for energy production and environmental applications.

### 1. Introduction

Global energy demand continues to increase due to population growth and economic expansion. Worldwide energy consumption reached 15 terawatts (TW) in 2010 and is expected to nearly double itself by 2050. Consequently, global energy shortages and the environmental damage caused by the combustion of fossil fuels will be huge challenges facing civilization over the next few decades. Research and development of renewable, clean, and carbon-neutral alternative energy resources is, thus, urgently required to reduce our dependence on fossil fuels.

Among the renewable energy resources, solar energy is the most abundant. Moreover, solar light, being free and green, is an ideal energy source for overcoming current environmental challenges. Considering that, in a single hour, the sun delivers energy sufficient for all human activities on the planet for an entire year, the harvesting of sunlight by artificial photocatalysts, and its conversion into solar fuels, is both viable and highly attractive.

Since Fujishima and Honda first reported the generation of H<sub>2</sub> through the photoelectrochemical splitting of water on TiO<sub>2</sub> electrodes under ultraviolet (UV) light in the early 1970s, the conversion of solar light to chemical energy using semiconductors has been explored as a key solution for energy production and pollutant degradation. However, a major challenge lies in designing an efficient sunlight-driven photocatalyst system.<sup>1</sup>

Solar fuels can take the form of hydrogen and

hydrocarbons such as methane and methanol. These products, which are considered as next-generation energy carriers, may be formed by photocatalytic water splitting and by photoreduction of CO<sub>2</sub> with water, respectively. Also, the photocatalytic process allows direct use of sunlight to decompose a wide range of organic pollutants, as photocatalysts can be excited by light to generate electron-hole pairs which can drive a variety of redox reactions.<sup>2</sup>

Much effort has been focused on the development of sunlight-driven photocatalysts in recent years; however, these materials still suffer from two fundamental efficiency bottlenecks: weak photon absorption and poor electron-hole pair separation. The development of highly efficient photocatalysts that absorb a large amount of solar energy and exhibit high charge separation is a key requirement for the conversion of solar radiation into chemical bond energy. Such a system could have a revolutionary impact on supplying our energy needs in a sustainable manner.

Recently, photocatalysts based on semiconductors with a hollow structure have received increasing research attention because of their unusual properties, such as high specific surface area, large sunlight absorption, and high electron-hole separation. Furthermore, hollow spheres allow multiple reflections of light within the interior cavity, which enhances the effectiveness of light utilization.

This review summarizes recent progress in the development of a variety of routes for the preparation of hollow structure photocatalysts, and highlights their application to fuel production and the decomposition of pollutants. We conclude with a concise overview of the current status, potential, and future development of hollow structure materials with a view toward improved performance in different photocatalytic redox applications.

Department of Chemical Engineering, Laval University, Quebec, G1V 0A8, Canada  
E-mail: trong-on.do@gch.ulaval.ca; Fax: +1-418-656-5993; Tel: +1-418-656-3774

## 2. Basic concept and current status in semiconductor photocatalysts

### 2.1. Concept of photocatalysis based on semiconductors

A photocatalytic system based on a semiconductor can be described by the band gap model, in which the valence band (VB), the highest occupied band, and the conduction band (CB), the lowest empty band, are separated by a band gap, a region of forbidden energies in a perfect crystal. An electron is excited to the CB and leaves a hole ( $h^+$ ) in the VB when the incident energy is equal to or larger than the band gap of the semiconductor, as depicted in **Figure 1**. The photoexcitation electron becomes utilised in a reduction reaction with an electron acceptor; for example, the reduction of protons to hydrogen, generation of an  $O_2^-$  radical, or  $CO_2$  reduction, but only if the CB minimum is located at a more negative potential than the electrochemical potential of the desired reaction. In the VB of the semiconductor, the photo-generated hole can also perform an oxidative reaction with an electron donor with oxidation potentials more negative than the VB maximum. Thus, the semiconductor is the most essential component in systems intended for the production of green fuel and other environmental applications.<sup>3</sup>

Photocatalysis occurs in the semiconductor via multiple steps, as illustrated in **Figure 2**. When the semiconductor is illuminated by a light source with higher energy than the band gap, an electron is excited to the CB, leaving behind a hole (Figure 2.1). Then, the thus-produced charge carriers migrate to the photocatalyst surface (Figure 2.2). The electron and hole recombine on the surface or in the bulk material while diffusing to the photocatalytic surface within a few nanoseconds (Figure 2.3). Simultaneously, the charge carriers that reach the semiconductor surface participate in the chemical conversion of the adsorbed reactants (Figure 2.4).<sup>4</sup> Therefore, it is widely accepted that greater the number of photo-generated carriers that are generated and reach the surface, the more efficiently the photoactive material will perform, and thus, photocatalytic performance is significantly influenced by the incident light absorption ability and charge separation efficiency of the catalyst. Particularly, a photocatalyst that exhibits a band gap around or larger than 3 eV will show restricted performance in the UV-region, as less than 5% of sunlight can be harvested by materials with a 3 eV band gap. Therefore, it should be noted that the number of electron-hole pairs generated is greater if the light absorption of semiconductor expands to the long wavelength region, i.e.,

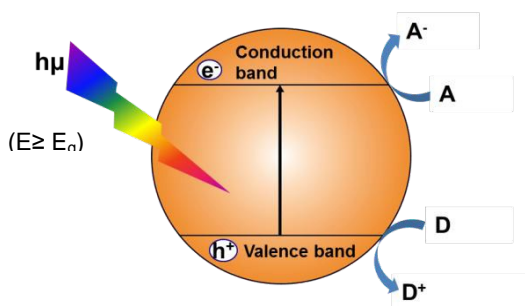


**Figure 1.** Electron hole generation under illumination in an inorganic photosystem; A: electron acceptor; D: electron donor.

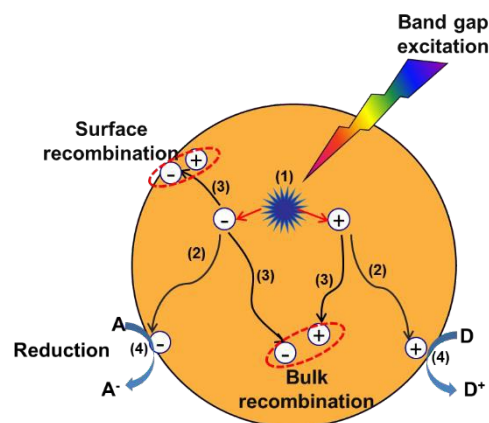


**Figure 2.** General processes in a semiconductor photocatalyst: 1) band gap excitation; 2) charge diffusion; 3) charge recombination; 4) chemical conversion.

a photocatalyst working under visible light will produce a higher quantity of photo-induced carriers in comparison with one irradiated by UV light.

In addition, the structure of the photosystem that utilizes the incident light is also an important factor in generating charge carriers effectively. For instance, nanotube structures reduce light loss due to the photon being trapped inside the structure by multiple light reflections with the wall. The number of photogenerated charge carriers, therefore, is significantly enhanced in comparison with the conventional morphology.<sup>5,6</sup> The second factor that has a strong influence on photoactivity is the number of the charge carriers reaching the surface to take part in chemical conversion. Recombination is often caused by a scavenger or crystalline defects which can trap the electron or the hole. Unfortunately, the vast majority of charge carriers produced recombine immediately after the band gap excitation event.<sup>7</sup> Based on the fundamental principles of semiconductor photocatalysis, an efficient photocatalyst must satisfy the light absorption and charge separation criteria simultaneously in order to exhibit high photoactivity.

### 2.2. Current advances in semiconductor photocatalysis

Light absorption ability and charge carrier separation are arguably the primary areas that need development in photocatalysis, and much research concerned with furthering this development has been recently reported. Band gap engineering, using nano-sized materials and utilization of nanocomposites are the major approaches to improving photocatalysts.

Electronic band structure is the key to solar chemical conversions. Doping is a method commonly used to extend the light absorption of wide band gap semiconductors to the longer-wavelength region. An absorption shift toward the red region is easy to realise in most doped semiconductors. The dopants can introduce localized electronic states, such as a donor level above the VB or an acceptor level below the CB in the forbidden band of wide band gap photocatalysts, which can narrow their band gaps. However, it is worth noting that the dopants may or may not cause enhancement to photocatalytic performance, depending on the doping-induced

change in the electronic band structure, as doped element(s) can function as charge recombination sites and reduce photoactivity.<sup>9</sup> Design and morphological control of the crystal facets of semiconductor photocatalysts with highly exposed active planes has been proved to be useful for the development of an efficient material.<sup>10</sup> Employing different facets with different surface atomic structures can narrow the band structure, as well as drive the photogenerated electron-hole pair in two distinct directions, leading to enhanced charge separation.<sup>11, 12</sup> An alternative approach using solid solution photocatalysts has emerged as a viable solution for the production of effective materials. GaN:ZnO, for instance, has shown potential for application in overall water splitting that originates from the strong visible light absorption, despite the wide band gap of both GaN (3.4 eV) and ZnO (3.2 eV). Recently, surface modification has attracted increasing attention. Mao *et al.* first proposed the synthesis of black TiO<sub>2</sub> which showed a high activity for hydrogen generation by hydrogenation under a 20 bar H<sub>2</sub> atmosphere for 5 days.<sup>13</sup> It is thought that surface disorder and oxygen vacancy are the main reasons for the strong visible/near infra-red light absorption. However, the oxygen vacancies in many cases have proven to jeopardize the photocatalytic performance as they can act as recombination sites.<sup>9, 14</sup>

In nano-sized materials, the smaller particle size exposes more active sites as well as lowering the travel path of the charge carrier to the surface. Quantum dots of metal chalcogens, such as CdS, CdSe, CdTe, and CuInS<sub>2</sub>, have already attracted a great attention due to their unique optical and electronic properties. Photogeneration of electron-hole pairs and their subsequent split into free carriers are the two key elements that directly determine the light response efficiency of a quantum dot material. However, it is not always accurate that the smaller the particle size, the higher the efficiency. A strong quantum confinement effect appears to increase the recombination probability of photogenerated electron-hole pairs. Although, small particle sizes indicate that charge carriers travelling to the surface have favourably short distances, this process requires a suitable concentration gradient or potential gradient (internal electric field) from the core of the particle to the surface, which has a close association with the morphology, structure and surface properties of nanostructured materials. In other words the internal electric field that helps separate electron-hole pairs in nanoscale photocatalysts is not sufficient to drive charge carriers in different directions and therefore leads to increased charge recombination.<sup>4, 15</sup>

Recently, the development of hybrid nanostructured photocatalysts has been shown to be the most efficient method to separate charge carriers and improve light absorption. A large number of excellent reviews have been published on the progress of composite photocatalysts that readers can refer for more detailed information<sup>16,17,18,19,20, 21,22,23,24,25,26,27</sup>. In general, the development of photo composites can be categorized into three primary approaches: co-catalysts, plasmonic photocatalysts, and heterojunction structures, as shown in Figure 3.

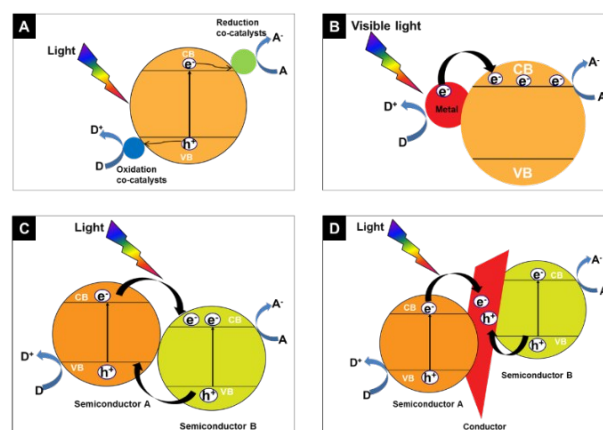


**Figure 3.** Typical example of the current developments in photo-composite materials; A) two separated co-catalysts; B) plasmonic photocatalysts; C) a type II photo composites; D) an all solid Z-scheme photocatalyst

A co-catalyst is a component that can only work together with a photocatalyst semiconductor. It is worth noting that co-catalysts play two main roles in the enhancement of photocatalytic performance: they promote charge separation and serve as reaction sites. Upon light irradiation, electrons migrate to the reduction sites to promote the reduction reaction, while the hole migrates to the oxidation co-catalyst to take part in the oxidation reaction, suppressing recombination and significantly enhancing the photoactivity, as shown in Figure 3A.<sup>28</sup> Noble metals are used as the reduction co-catalyst.<sup>29</sup> The different properties of the noble metal and n-type semiconductor cause a barrier (Schottky barrier) and space charge region (also called the depletion layer) as a result of the electron transfer process from the semiconductor near the metal-semiconductor interface to the metal when they come into contact. Moreover, the charge redistribution creates an internal electric field which drives the photogenerated electron and hole to the bulk semiconductor and metal, respectively. Under the successive photoexcitation of the semiconductor, a large number of electrons accumulate in the semiconductor, making them hot enough to transfer to the metal. Using noble metal-free co-catalysts has also received much attention over recent years. Inexpensive and abundant nano-sized materials formed from transition metals (Ni, Co, Cu) and transition metal compounds, such as transition metal oxides, metal hydroxides, and metal sulfides, have been shown to be efficient co-catalysts for reduction reactions. These co-catalysts show activities comparable to that of Pt, which is attributed to the effective charge separation caused by efficient electron transfer from the semiconductor to the co-catalyst.<sup>30, 31</sup> Moreover, carbonaceous nanomaterials, such as carbon nanotubes and graphene, have been shown to promote charge carrier separation. Because of their high electrical conductivity, which is caused by sp<sup>2</sup>-hybridized carbon atoms, they can function as a co-catalyst that accepts photogenerated electrons from the semiconductor photocatalyst, leading to significantly enhanced charge separation.<sup>32,33, 34</sup> In the same manner, photogenerated holes are also attracted by oxidation co-catalysts to enhance the oxidation reaction. To extract the holes, their band levels

should be higher than that of the light-harvesting semiconductor. Generally, metal oxides like  $\text{MnO}_x$ ,  $\text{FeO}_x$ ,  $\text{CoO}_x$ ,  $\text{NiO}_x$ ,  $\text{CuO}_x$ ,  $\text{RuO}_2$  and  $\text{IrO}_2$  are selected for oxidation co-catalysts.<sup>35</sup> Very recently, carbon quantum dots, a novel class of carbon nanomaterials, have been shown to promote the rate of water oxidation in the decomposition of pure water under solar light. Because of their unique photo-induced electron transfer, photoluminescence, and electron reservoir properties, photocatalyst-based carbon quantum dots not only facilitate charge separation, but are also promising as efficient and full sunlight absorption materials.<sup>36, 37</sup>

Localized surface plasmon resonance (LSPR) has been applied in the photocatalytic field and has attracted considerable attention over the past few years. The presence of plasmon metal nanoparticles shifts the light absorption to the long wavelength region, caused by free electron oscillation on the metal particle surface when the frequency of photons matches the natural frequency of these electrons. Through the LSPR excitation of plasmonic metals, energetic electrons are produced at the metal surface. These energetic electrons remain in the excited "hot" state for up to 0.5–1 ps; they gain enough energy under visible light illumination to facilitate the transfer to the conduction band of semiconductor and participate in the chemical conversion, as shown in **Figure 3B**. Cu, Ag, and Au nanoparticles generally reveal a strong photoabsorption of visible light because their surface plasmon exhibits the absorbance at approx. 580, 400 and 530 nm, respectively. However, nanostructured copper and silver are easily oxidized, whereas Au nanoparticles display the chemical stability. Furthermore, it is noted that the photocatalytic performance of plasmonic photocatalysts is influenced by many factors such as the nanoparticle size, the shape and the surrounding environment.<sup>35, 38</sup>

**Figures 3C and 3D** show the typical semiconductor alignment in composite materials that have been shown to cause a remarkable improvement in photoactivity. Not only is light absorption improved in the composite photosystem, but also the electron-hole separation, which is enhanced by electron and hole transfer at the semiconductor-semiconductor junction (type II semiconductor) or semiconductor-conductor-semiconductor (all solid Z-scheme).<sup>35</sup> In type II semiconductors, the hole-electron separation highly depends on the electric field at the interface. In the other words, the strong internal electric field promotes efficient charge separation. However, the redox ability of the charge carriers usually decreases after the charge transfer processes. The Z-scheme is proposed to address the problem through mimicking the natural photosynthesis system. Thus, using the Z-scheme has some advantages, such as maintaining charge carrier energy levels and harvesting visible-light to archive the overall reaction. For example, an all solid Z-scheme has been developed by inserting the conductor between two semiconductors to form ohmic contact with low contact resistance. As a consequence, electrons from the CB of semiconductor A can directly recombine with holes from semiconductor B (see Fig. 3D).<sup>35</sup>

### 3. Hollow structure materials

#### 3.1. Advantages of hollow structure photocatalytic materials

The emergence of hollow structure materials has provided a new opportunity to design high-power materials for diverse applications such as batteries, biomaterials, and heterogeneous catalysts. Hollow structures possess unique properties. For example, the large fraction of empty space in hollow structures has been used to load and control photocatalytic systems for particular materials, such as genes, peptides, and biological molecules. Their structural features and connection conductivity reduce the diffusion distance of the electrolyte,

and therefore enhance their suitability as energy storage materials. In addition, hollow catalytic materials have a higher surface area, which is a valuable property for heterogeneous catalysts.<sup>39</sup>

In the photocatalytic field, hollow structures are a good choice for morphology construction in artificial photosystems. Firstly, hollow photocatalysts are composed of nanoparticles, and therefore exhibit significantly improved charge separation. It is worth noting that reducing the particle size to nanoscale has considerable influence on electron-hole pair separation due to the large surface area, lower travel path, and the high density of active sites. However, the small space in the nano-size particles enables the photo-generated charge carriers to more easily recombine. Hence, the development of photocatalysts should exploit the advantages of nanoscale materials while limiting their negative aspects. Structural forms that combine micro-scale and nano-sized powdered catalysts are a potential way to meet both requirements.<sup>15, 40</sup> Furthermore, hollow structures exhibit porosity, which reduces the diffusion length and improves the accessibility of active sites by the reactants.<sup>41</sup> Additionally, the multiple reflections within the hollow cavity enhance efficient use of the light source, leading to the production of more photogenerated charge carriers.<sup>42, 43</sup> Consequently, hollow photocatalysts may overcome the current challenges associated with light adsorption and charge separation in the

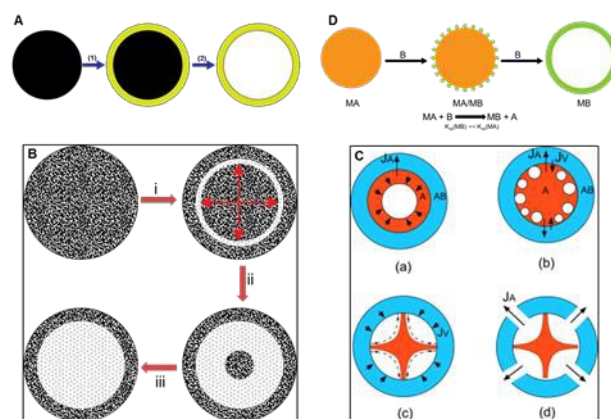


**Figure 4.** Schematic illustration of the formation the hollow structure; A) template strategy; B) Ostwald ripening; C) Kinkendall effect; D) ion exchange

development of photocatalytic semiconductors

### 3.2. General strategies for constructing hollow structure photocatalysts

The formation of hollow materials is based on two main approaches: templated and template-free. **Figure 4A** shows a schematic illustration of hollow structure formation based on a hard support. The desired material is coated onto the sacrificial core prior to removal of the core by chemical etching or thermal treatment. Interaction between the precursors and the supported surface prompts the loading of precursors onto the core surface. Then, the hollow structure is generated after removal of the core.

Polymers, silica, and carbon colloidal spheres are commonly employed to construct hollow photocatalysts because their negative surface charge facilitates interaction between the core and precursors through electrostatic forces. In the case of  $\text{SiO}_2$  spheres, the hollow spheres are released after removing the  $\text{SiO}_2$  core by chemical etching with  $\text{NaOH}$ ,  $\text{HF}$ , or  $\text{NH}_4\text{HF}_2$ , while thermal treatment is used to obtain the hollow material when polymer or carbon spheres are employed as the template.

By contrast, template-free synthesis relies on the physical and/or chemical properties of the material during the synthesis processes. Ostwald ripening, Kirkendall effect, and ion exchange, are the prevailing strategies used to obtain hollow structures, as depicted in **Figure 4B** and **Figure 4C**.

In principle, Ostwald ripening can be thought of as the consequence of a single phase system being put into a two-phase metastable state. The inner phase that has higher energy will move to the stable outer surface through ripening, resulting in the hollow structure.<sup>44</sup>

As an alternative method, Smigekas and Kirkendall demonstrated the movement of an interface between a diffusion couple as a result of the different diffusion rates of the two species at an increased temperature. This phenomenon, now defined as the Kirkendall effect, is proposed to explain the void formation in metal oxide hollow structures. At the higher temperature, if the outward diffusion rate is faster than that of inward, an internal space will be formed.<sup>45</sup> In another method, a hollow material can be obtained through ionic exchange reactions due to differences of solubility product constants and diffusion rate as depicted in **Figure 4D**.<sup>46</sup> The formation of hollow metal sulfides can usually be explained by this phenomenon.

The works above indicates that diverse hollow structures can be produced based on hard template and/or template-free strategies. Utilization of a sacrificial core can facilitate the construction of materials with uniform morphology, hollow dimensions, and wall thickness. However, core removal by chemical etching or thermal treatment is a disadvantage of this method because the phase structure or surface properties can be impacted by high temperature and chemical reactions. In contrast, the evolution of hollow materials through template-free approaches preserves surface properties. Additionally, the hollow dimensions can be controlled by the

fabrication conditions. However, the conditions suitable for obtaining the hollow structure, and the non-uniformity of the as-prepared hollow structures, limit the development of semiconductors based on template-free routes. Therefore, the selection of a suitable approach to designing hollow structure photocatalysts greatly depends on the desired photocatalysts and used precursors.

## 4. State-of-the-art in the development of hollow photocatalysts

There have been many advances in hollow photocatalysts recently, and the development of this type of construction can generally be divided into two approaches: single component and composite hollow photocatalysts. The former route has been intensively studied over the last ten years, and has two main branches: single-shell and multiple-shell hollow structures. However, the composite approach has recently received increasing attention.

### 4.1. Single-component hollow photocatalysts

#### 4.1.1. Single-shell photocatalysts.

Single-shell hollow photocatalysts are the most well-known hollow structure. Their unusual architecture and simple fabrication method make them potential candidates for robust photocatalysts. In general, two routes are accepted for the development of hollow photocatalytic material: hard template and template-free, as discussed above. In the template approach, silica, carbon colloids, and polymer spheres are typical templates for hollow synthesis. The template-free route is based on physical phenomena, such as Ostwald ripening, the Kirkendall effect, and ionic exchange, as listed in **Table 1**. Since single-shell photocatalysts have been showed the significant improvement in the photoreactions, below we will therefore select several well-designed nanostructured hollow material as examples.

For instance, Sun *et al.* reported  $\text{g-C}_3\text{N}_4$  hollow sphere photocatalysts for hydrogen production under visible

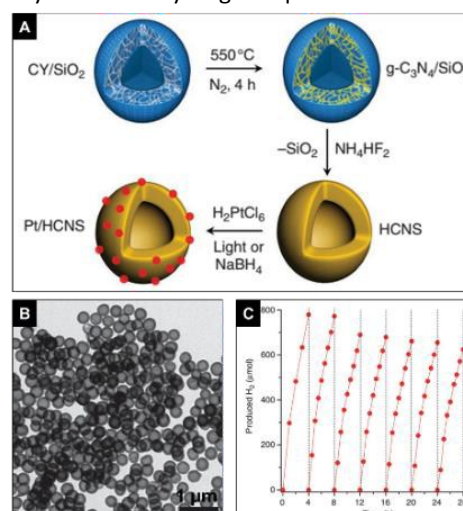


**Figure 5.** A) Schematic illustration of the procedure for synthesis of  $\text{C}_3\text{N}_4$  hollow spheres; B) TEM image of  $\text{C}_3\text{N}_4$  hollow spheres; C) photoactivity for hydrogen evolution of  $\text{C}_3\text{N}_4$  hollow spheres.

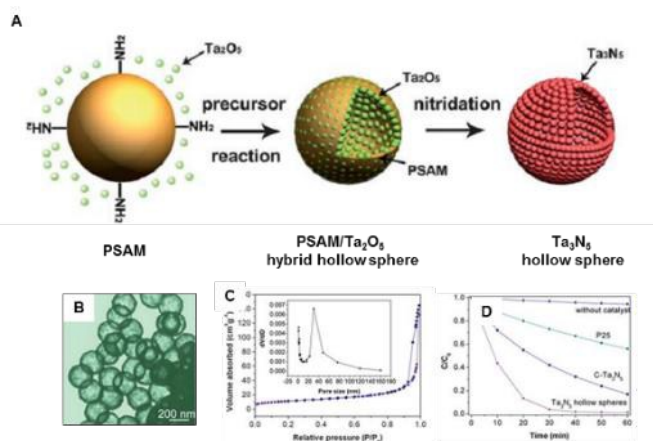


**Figure 6.** A) Schematic illustration of the synthesis of  $\text{Ta}_3\text{N}_5$  hollow spheres; B) TEM image of hollow  $\text{Ta}_3\text{N}_5$ ; C) nitrogen adsorption-desorption isotherm and pore size distribution of the  $\text{Ta}_3\text{N}_5$  hollow microspheres; D) photocatalytic evaluation of  $\text{Ta}_3\text{N}_5$  hollow spheres.

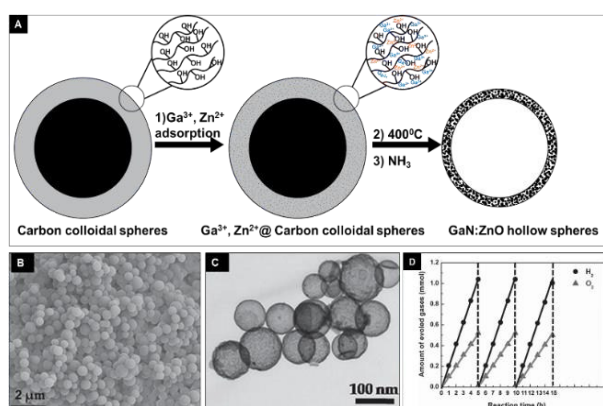


**Figure 7.** A) Schematic illustration of GaN:ZnO hollow photocatalyst fabrication; B) SEM image of as-prepared carbon colloidal spheres; C) TEM image of GaN:ZnO hollow spheres; D) photoactivity of GaN:ZnO hollow spheres in water splitting under visible light.

illumination with an apparent quantum yield (AQY) of approximately 7.5% at 420.5 nm.  $\text{g-C}_3\text{N}_4$  was prepared from cyanamide, which was loaded into silica spheres containing meso pores as the hard template, as described in **Figure 5**. The resulting hollow  $\text{g-C}_3\text{N}_4$  is formed after removing the silica core by chemical etching. According to the literature, the hollow spheres showed a remarkable enhancement of photoabsorption in the 440–550 nm range, which was attributed to multiple reflections within the hollow structure. Moreover, it is worth noting that the number of defects decreases with the shell thickness to the nano range. For these reasons, the amount of hydrogen generated in the  $\text{g-C}_3\text{N}_4$  hollow structure was much higher than that of bulk  $\text{g-C}_3\text{N}_4$  by a factor of 25. Furthermore, the catalyst showed high stability over seven cycles.<sup>47</sup> It can be said that cyanamide and silica nanospheres are good choices for the design of the  $\text{C}_3\text{N}_4$  hollow structure due to two main reasons: Firstly, silica spheres are a thermally stable hard template. Hence, development of the porous structure on the surface of silica spheres is feasible. On the other hand, cyanamide possesses the low melting temperature (44 °C), which promotes loading of this precursor into the porous structure, leading to the formation of bulk  $\text{C}_3\text{N}_4$  through thermal treatment. As a result,

the hollow structure is released after core removal. An alternative sacrificial support strategy is the utilization of polymer spheres. This type of support offers uniform morphology, a simple fabrication method, and ease of surface modification. Using this methodology the hollow photocatalyst can be generated by coating with a layer of photocatalyst or precursor before removing the polymer core. Gao reported the fabrication of  $\text{Ta}_3\text{N}_5$  hollow microspheres based on poly(styrene-co-acrylamide) (PSAM) colloidal spheres as a sacrificial support (**Figure 6**). Because of the covalent bond formation between  $\text{Ta}(\text{OEt})_5$  and the amine-functionalized polymer, the  $\text{Ta}_2\text{O}_5$  precursor is easily loaded onto the template. The hollow structure of  $\text{Ta}_3\text{N}_5$  is formed under nitridation conditions in  $\text{NH}_3$  at high temperature, producing a material with a high specific surface area and high volume. By the combination of many unique properties, such as their meso-microporous structure,  $\text{Ta}_3\text{N}_5$  hollow microspheres exhibit photoactivity improvement in the degradation of pollutants.<sup>48</sup>

Employing carbon colloidal spheres as a sacrificial support has also received considerable attention for hollow structure preparation over the last decade. Due to the robust electrostatic interaction between metal cations and the negative charge on the carbonaceous sphere surface, high-density absorption of cation species occurs, followed by the release of the hollow structure by removing the carbon core through calcination. Also, the hollow photocatalyst can also be produced by one-pot synthesis approach, in which a mixture of metal salt and carbon sphere precursors are put in a sealed autoclave at a precise temperature. The hollow spheres are then produced by calcination to remove the carbon material. Thereby, the development of carbon colloidal spheres led to a significant surge in the development of metal oxide hollow photocatalysts.<sup>49</sup>

For example, Li *et al.* reported a GaN:ZnO hollow photocatalyst constructed on carbon colloidal spheres for hydrogen generation (**Figure 7**). In this preparation, a mixture of  $\text{Ga}^{3+}$  and  $\text{Zn}^{2+}$  is adsorbed onto a carbon colloidal sphere surface in DMF solvent. Mixed oxide GaN:ZnO hollow spheres were obtained by calcination to combust the carbon core, followed by nitridation in ammonia. It should be noted that the nitridation temperature required decreased significantly due to the higher surface energy and short atomic diffusion distance in the hollow structure. Furthermore, the as-prepared material also showed a high surface area (up to  $114.4 \text{ m}^2 \cdot \text{g}^{-1}$ ) attributed to the small grain size (5–10 nm) of GaN:ZnO constructed on the hollow structure. As a consequence, the GaN:ZnO hollow photocatalyst showed excellent photoactivity in hydrogen generation with a quantum yield (QY) of 17% at 400 nm illumination.<sup>50</sup> Employing carbon colloidal spheres usually produces high surface photocatalysts due to pores being formed during the combustion of the carbon core. In addition, the simple preparation route and low cost of carbon sphere precursors (usually glucose or sucrose) have made this method very popular for the synthesis of hollow metal oxide structures.

In addition to the template approach, routes based on the physical phenomena of Ostwald ripening, the Kirkendall effect, and ion exchange have proved to be an efficient advance in fabricating hollow single-shell structures.

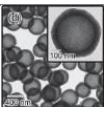
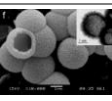
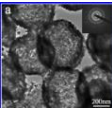
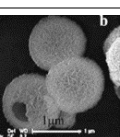
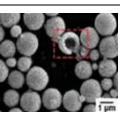
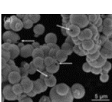
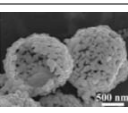
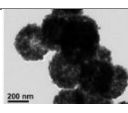
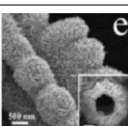
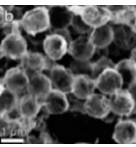
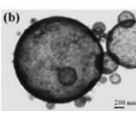
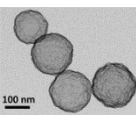
With Ostwald ripening, Cao *et al.* produced TiO<sub>2</sub> hollow spheres by treating solvothermal amorphous titania microspheres, as shown in **Figure 8**. The resulting hollow structure is attributed to the crystallization from amorphous titania to anatase nanocrystals using metastable ammonium titanate as the seed for initiating the Ostwald ripening process.<sup>62</sup> In all the photocatalyst fabrications based on the Ostwald ripening approach, the formation of a biphasic in which the outer phase is more stable than the inner phase is the paramount condition. The inner phase with higher energy diffuses into the outer phase during the ripening process, and, as a result, the phases have different energies. Moreover, the reaction time is also the critical parameter for the complete formation of the hollow spheres. Unlike Ostwald ripening, the formation of a hollow photosystem by the Kirkendall effect occurs from the movement of the interface between a diffusion couple at increased temperature. For instance, Ibáñez reported excellent work on the formation of uniform CdS hollow spheres through the Kirkendall effect from Cd particles as described in Figure 9A. The evolution of the hollow CdS originates from the faster diffusion rate of Cd than the excess sulfur in the reaction media through the formed CdS shell, which releases the space inside.<sup>63</sup> Another template-free method for the formation of hollow structure photocatalysts is ion exchange, which is based on the difference in the stability constant of the product. For instance, Chen *et al.* introduced the formation of hollow structure Bi<sub>2</sub>WO<sub>6</sub> from BiOBr through anion exchange. The critical parameter for the formation of Bi<sub>2</sub>WO<sub>6</sub> is the solubility product constant  $K_{sp}$  of Bi<sub>2</sub>WO<sub>6</sub>, which is minuscule in comparison to that of BiOBr. For this reason, the replacement of WO<sub>4</sub><sup>2-</sup> is thermodynamically favourable, as depicted in **Figure 9B**.<sup>55</sup>

#### 4.1.2. Multi-shell hollow photocatalysts

Multi-shell hollow structure photocatalysts have recently attracted increasing attention because of their remarkable advantages. By virtue of the nanoparticle assembly, multi-shell hollow photocatalysts possess not only low density and high surface area, but also abundant inner spaces that overcome the mass transport problem. Multiple reflections within shells improve light absorption, leading to the generation of more photo charge carriers, as illustrated in **Figure 10A**.

Qi *et al.* produced triple-shelled CeO<sub>2</sub> hollow microspheres by employing a carbonaceous sacrificial template, as illustrated in **Figure 10B and 10C**. The adsorption of Ce<sup>3+</sup> during the fabrication process in the presence of urea as the alkali agent facilitates deep penetration of Ce<sup>3+</sup> before thermal treatment in order to obtain the multi-shelled hollow CeO<sub>2</sub> structure. The prepared CeO<sub>2</sub> is constructed from nanoparticles of several nanometres in size and shows a high surface area in comparison with single-shelled and commercial CeO<sub>2</sub>. Consequently, the material shows good performance in photo-induced oxygen generation, approximately 12 times higher than normal CeO<sub>2</sub> nanoparticles under UV irradiation.<sup>64</sup>

**Table 1.** List of single shell hollow photocatalysts

Type	Morphology	Strategy	Application	Ref.
TiO <sub>2</sub>		Hard template - SiO <sub>2</sub> spheres	RhB degradation	51
TiO <sub>2</sub>		Template-free - Ostwald ripening	Phenol degradation	42
ZnO		Hard template - carbon colloidal spheres	Degradation of RhB	52
ZnO		Template-free - Ostwald ripening	Degradation of organic dye	53
Bi <sub>2</sub> WO <sub>6</sub>		Template-free - Ostwald ripening	Degradation of RhB	54
Bi <sub>2</sub> WO <sub>6</sub>		Anion exchange	Reduction of CO <sub>2</sub>	55
BiMoO <sub>6</sub>		Hard template - carbon colloidal spheres	Degradation of phenol	56
Bi-doped ZnS		Cation exchange	Hydrogen generation	57
WO <sub>3</sub>		Template-free - Kirkendall effect	Degradation of RhB	58
TaO <sub>3</sub>		Hard template - PS	Hydrogen generation	59
BiFeO <sub>3</sub>		Template-free - Kirkendall effect	Degradation of RhB	60
LaTiO <sub>2</sub> N		Hard template - carbon colloidal spheres	Hydrogen production	61



**Figure 8.** Formation of  $\text{TiO}_2$  hollow spheres by Ostwald ripening; A). Formation of  $\text{TiO}_2$  hollow spheres from amorphous titania; B,C,D,E) SEM images of each step.<sup>62</sup>

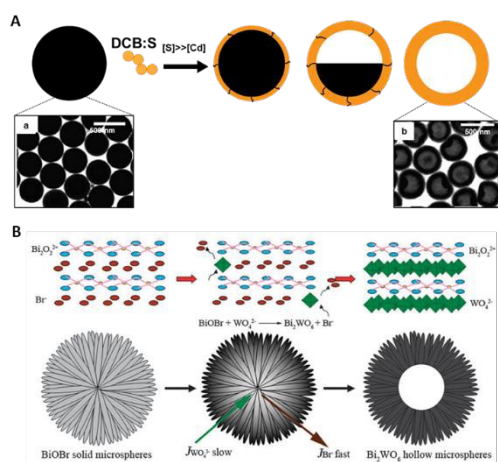


**Figure 9.** A) The formation of CdS spheres through the Kirkendall effect: a) Cd particles; b) CdS hollow spheres.<sup>63,64</sup> B) The formation of  $\text{Bi}_2\text{WO}_6$  through the anionic exchange mechanism.<sup>65</sup>

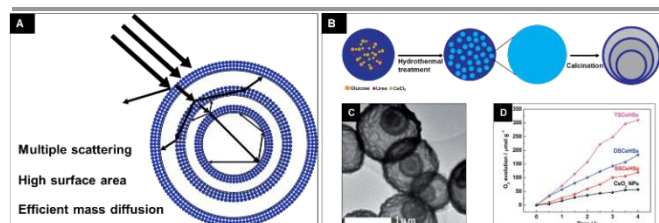


**Figure 10.** Multiple light absorption in a multi-shell hollow structure; B) schematic illustration of  $\text{CeO}_2$  triple-hollow spheres;<sup>65</sup> C) TEM image of triple-hollow  $\text{CeO}_2$ ; D) photoactivity for oxygen evolution of triple-hollow  $\text{CeO}_2$  spheres.<sup>65</sup>

In another recent work, silica spheres were employed as the template for fabrication of multi-shelled  $\text{TiO}_2$ . The number of silica layers and interstitial  $\text{TiO}_2$  layers dictated the number of shells. Similarly to the triple-shelled  $\text{CeO}_2$ , the triple-shelled hollow  $\text{TiO}_2$  showed an improvement in photocatalytic activity due to its high surface area (up to  $171 \text{ m}^2 \cdot \text{g}^{-1}$ ) and facile electrolyte diffusion.<sup>65</sup>

These recent publications prove that multiple-shell hollow photocatalysts show significantly improved photoactivity, mainly due to the multi-reflection of incident light and the high density of active sites. Hard templates are suitable for constructing this type of hollow structure. Nevertheless, the

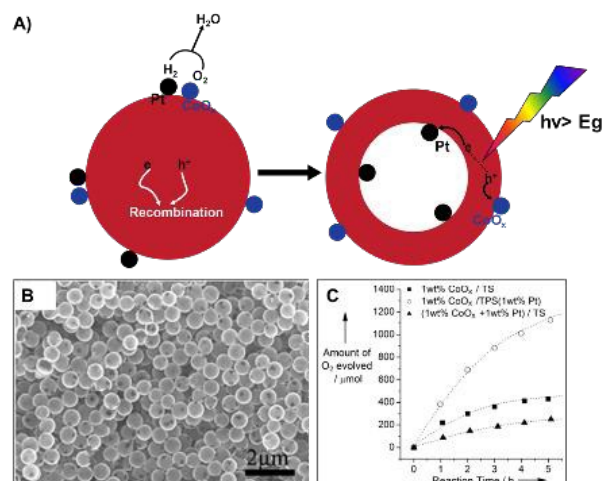


**Figure 11.** A) Illustration of the photoactivity improvement in a separated co-catalyst with a hollow structure; B) SEM image of hollow  $\text{Pt}/\text{Ta}_3\text{N}_5/\text{CoO}_x$  photoactivity for oxygen generation under visible light of hollow  $\text{Pt}/\text{Ta}_3\text{N}_5/\text{CoO}_x$ .<sup>77</sup>

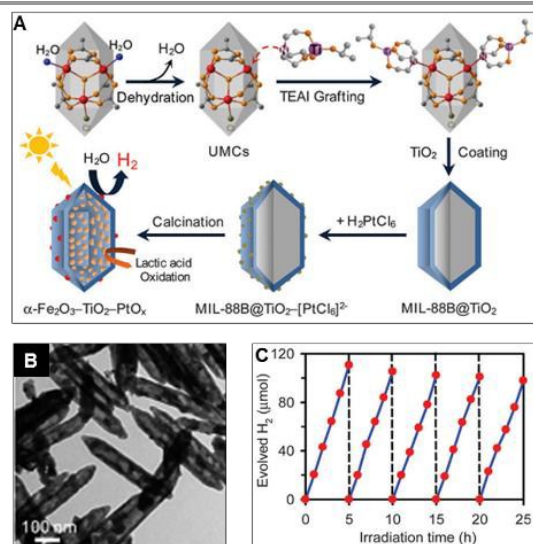


**Figure 12.** A) Schematic illustration of  $\text{Fe}_2\text{O}_3\text{-TiO}_2\text{-PtO}_x$  preparation from MIL-88B; B) TEM images of hollow  $\text{Fe}_2\text{O}_3\text{-TiO}_2\text{-PtO}_x$ ; C) amount of hydrogen generated under visible light irradiation.<sup>78</sup>

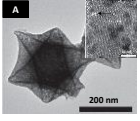
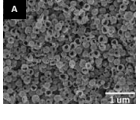
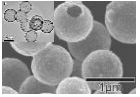
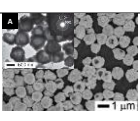
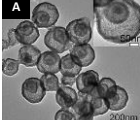
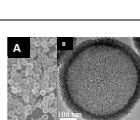
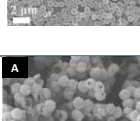
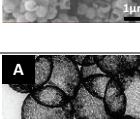
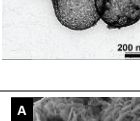
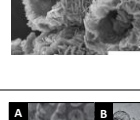
preparation and control of shell number in multi-hollow structures requires strict synthesis conditions.

#### 4.2. Composite hollow photocatalysts

A composite photocatalyst system could address the key issues for improving photocatalytic activity, i.e., light adsorption and good charge carrier separation. Therefore, the design of a photocomposite system based on a hollow structure is a promising approach because of the combination of the advantages of the hollow structure and the photocomposite. A large number of hollow composite photocatalysts have been reported over recent decades, as listed in **Table 2**. Here, we arrange the hollow composite photocatalysts into three main sub-sections: two separated co-catalysts, plasmonic catalysts, and heterojunction hollow photocatalysts.

##### 4.2.1. Two separated co-catalysts hollow photocatalysts

Table 2. List of hollow composite photocatalysts

Type	Morphology	Strategy	Application	Ref.
Fe <sub>2</sub> O <sub>3</sub> /Fe-doped TiO <sub>2</sub> /Pt		Hard template – MIL 101	Hydrogen production	66
Au/TiO <sub>2</sub>		Hard template - SiO <sub>2</sub> spheres	Methylene blue degradation	67
Ag/TiO <sub>2</sub>		Hard template – Carbon colloidal spheres	Degradation of RhB	68
Ag/AgI		Template-Free - Kirkendall effect	Hydrogen generation	69
Au/CeO <sub>2</sub>		Hard template- Carbon colloidal spheres	Reduction of p-nitrophenol	70
TiO <sub>2</sub> /Au/TiO <sub>2</sub>		Hard template - SiO <sub>2</sub> spheres	CO oxidation, H <sub>2</sub> production, nitrophenol reduction	71
Fe <sub>3</sub> O <sub>4</sub> /TiO <sub>2</sub>		Hard template - PSA	RhB degradation	72
ZnO/TiO <sub>2</sub>		Hard template - PS	Rhodamine 6G degradation	73
CdMoO <sub>4</sub> @CdS		Template free- ion exchange	RhB degradation	74
GO/TiO <sub>2</sub>		Hard template - SiO <sub>2</sub> spheres	RhB degradation	75
Au@r-GO/TiO <sub>2</sub>		Hard template - SiO <sub>2</sub> spheres	RhB degradation	76

The presence of co-catalysts provides active sites for

photoreactions, imparts overpotential to the semiconductor surface, lowers activation energy, and also improves charge separation and suppresses photo-corrosion. In addition, the Schottky barrier formed at a semiconductor and metal co-catalyst interface shifts the metal Fermi level towards negative values, which facilitates electron trapping. Hence, metal or metal oxide co-catalysts not only present reduction sites and serve as electron sinks, but also allows separation of the photogenerated carriers. Similarly, the existence of oxidation co-catalysts is an essential requirement for the transfer of

photogenerated holes to the surface, especially in hole reactions, such as photo-induced oxygen generation.<sup>35</sup> For this reason, the simultaneous presence of dual co-catalysts on the semiconductor is proposed to have a synergistic effect on charge separation and surface reactions. However, the development of separated co-catalyst systems remains difficult by conventional fabrication methods. These traditional strategies use impregnation or photodecomposition methods that are not selective for the deposition of co-catalysts.

Hollow structure construction has been demonstrated as appropriate for the co-catalyst approach. As shown in **Figure 11**, a Ta<sub>3</sub>N<sub>5</sub> hollow structure with two co-catalysts located on opposite sides of a Ta<sub>3</sub>N<sub>5</sub> wall was constructed by employing silica spheres as a hard template. Platinum is deposited on the silica spheres as the reduction co-catalyst before coating with a layer of Ta<sub>2</sub>O<sub>5</sub> and deposition of cobalt oxide (CoOx). Afterward, the as-prepared material is treated in an NH<sub>3</sub> atmosphere and the silica core is removed by chemical etching in order to obtain the desired photocatalyst. Accordingly, the dual co-catalysts present on the Ta<sub>3</sub>N<sub>5</sub> show significantly enhanced oxygen evolution generation activity under visible irradiation in comparison with the single catalyst and the two co-catalysts by a factor of three and five, respectively (**Figure 11C**). This remarkable activity can be ascribed to the co-existence of dual co-catalysts separately located on Ta<sub>3</sub>N<sub>5</sub>.<sup>77</sup> Dekrafft developed a new hollow structure photocatalyst based on metal-organic framework (MOF) nanocrystals, namely MIL-101, with Fe<sub>2</sub>O<sub>3</sub> and Pt nanoparticles serving as two co-catalysts deposited on TiO<sub>2</sub>. The formation of this material is based on the interaction between Lewis acid sites (Fe<sup>3+</sup>) in the MOF structure and the Lewis basicity of the titanium precursor. The loading of TiO<sub>2</sub> on MIL-101 is facilitated by hydrolysis before deposition of the Pt as second co-catalysts. Recently, our group developed a hollow TiO<sub>2</sub> structure with Fe<sub>2</sub>O<sub>3</sub> and platinum oxide (PtO<sub>x</sub>), which serve as two separate co-catalysts deposited on opposite sides of a hollow wall, illustrated in **Figure 12**. Coating with TiO<sub>2</sub> is based on the interaction between Lewis acid sites exposed on unsaturated metal centres of dehydrated MIL-88B and the Lewis basic titanium precursor. The hollow TiO<sub>2</sub> co-catalyst material is subsequently generated by calcination. The amount of hydrogen produced using this material demonstrates that the prepared photosystem has efficient photoactivity.<sup>78</sup>

#### 4.2.2. Plasmonic hollow photocatalysts.

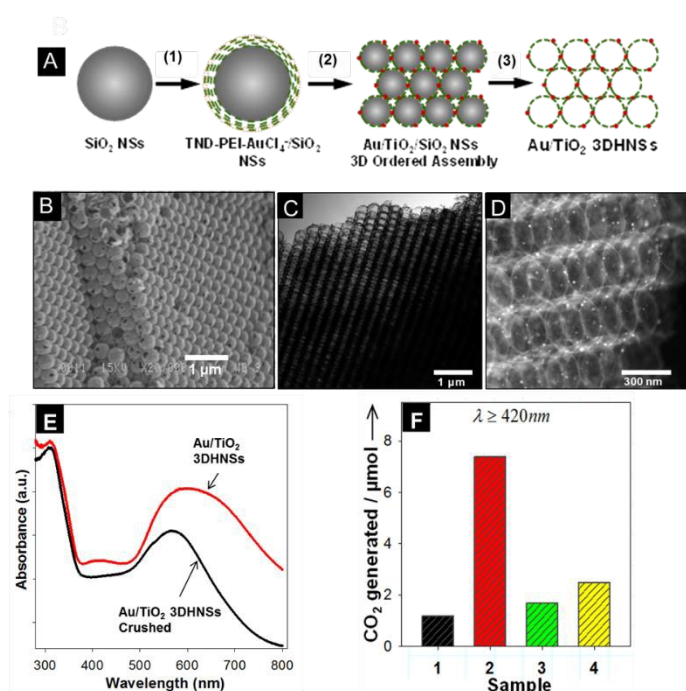


**Figure 13.** A) Schematic illustration of the fabrication of Au/TiO<sub>2</sub>-3DHNSs; B) SEM, and C,D) TEM and STEM of Au/TiO<sub>2</sub>-3DHNSs; E) UV-Vis spectroscopy of Au/TiO<sub>2</sub>-3DHNSs; F) amount of CO<sub>2</sub> generated under visible light illumination, 1: Au-TiO<sub>2</sub> (P25); 2: Au/TiO<sub>2</sub>-3DHNSs; 3: crushed Au/TiO<sub>2</sub>-3DHNSs; 4: disordered Au/TiO<sub>2</sub>-HNSs.

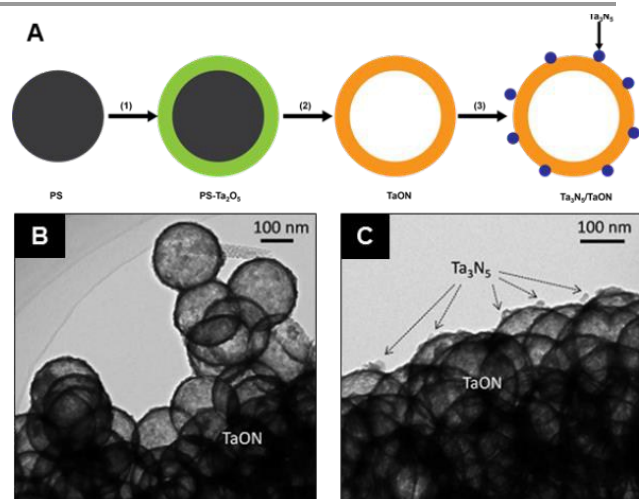


**Figure 14.** A) Schematic illustration of the production of a Ta<sub>3</sub>N<sub>5</sub>/TaON hollow composite photocatalyst; B, C) TEM images of TaON and Ta<sub>3</sub>N<sub>5</sub>/TaON, respectively.

An important strategy for the development of composite photocatalytic systems is the exploitation of surface plasmon resonance in noble metals such as Au and Ag. A hollow structure plasmonic composite displays improved photo-activity compared with normal plasmonic nanocomposites due to the increased contact between the metal nanoparticles and the support.<sup>79</sup>

Very recently, our group has developed three-dimensional photonic hollow structure Au/TiO<sub>2</sub>. Based on the layer-by-layer (LBL) self-assembly technique, a three-dimensional ordered assembly of thin-shell Au/TiO<sub>2</sub> hollow nanospheres (HNSs) was fabricated, as illustrated in **Figure 13**. Due to the hydrophilic surface of the silica sphere, polyethylenimine (PEI) is attracted through electrostatic interaction and makes the

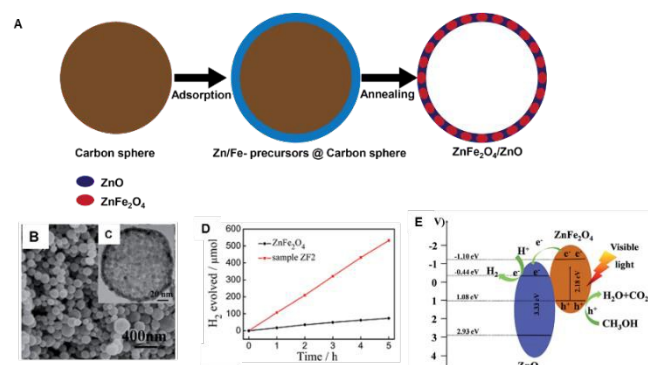


**Figure 15.** A) formation of hollow structure ZnFe<sub>2</sub>O<sub>4</sub>/ZnO; B,C) SEM and TEM images, respectively, of hollow structure ZnFe<sub>2</sub>O<sub>4</sub>/ZnO; C) amount of hydrogen generated on hollow structure ZnFe<sub>2</sub>O<sub>4</sub>/ZnO; D) amount of CO<sub>2</sub> generated under visible light illumination, 1: Au-TiO<sub>2</sub> (P25); 2: Au/TiO<sub>2</sub>-3DHNSs; 3: crushed Au/TiO<sub>2</sub>-3DHNSs; 4: disordered Au/TiO<sub>2</sub>-HNSs.

surface charge positive. Then, titanium nano-disks with negative surface charge are deposited by the LBL technique via electrostatic interaction with PEI, followed by loading with HAuCl<sub>4</sub> to produce TND-PEI-AuCl<sub>4</sub>/SiO<sub>2</sub>. Assembly of TND-PEI-AuCl<sub>4</sub>/SiO<sub>2</sub> is performed by centrifugation at low speed, followed by calcination to obtain the Au/TiO<sub>2</sub>/SiO<sub>2</sub> ordered structure. The silica core is then removed by NaOH solution to release the ordered Au/TiO<sub>2</sub> hollow structure. This unique high surface structure shows a photonic stop band at 550–620 nm, which matches the surface plasmon resonance absorption of gold nanoparticles. These ordered Au/TiO<sub>2</sub> hollow spheres show remarkable activity in the decomposition of isopropanol compared to the same photocatalyst without the ordered structure.<sup>80</sup>

#### 4.2.3. Hollow heterojunction photocatalysts.

It can be argued that the development of heterojunction structure photocatalysts is the most critical approach to developing efficient photocatalytic materials, as the fundamental requirements of photocatalytic materials, such as high crystallinity, efficient light absorption, and proper charge separation, can be satisfied simultaneously by combining two or many semiconductors. Consequently, numerous reports have been published on the development of heterojunction photocatalysts. However, the conventional method of photo composite fabrication is the mixing of many individual semiconductors, which leads to small surface areas and an ineffective incident light utilization. The fabrication of composite photocatalysts based on a hollow structure overcomes these drawbacks and shows promise as a good candidate for production of an efficient artificial photosystem.

To date, a variety of composite hollow photocatalysts have been reported. For instance, Ta<sub>3</sub>N<sub>5</sub> quantum dots were applied *in situ* to a TaON hollow structure wall that was produced using a polymer sphere template, as illustrated in **Figure 14**. The composite photocatalyst showed excellent activity for oxygen generation due to the close contact between the Ta<sub>3</sub>N<sub>5</sub> and the TaON hollow spheres, with apparent quantum efficiencies up to 67% under 420 nm light.<sup>81</sup>

In another work, a hollow heterojunction system comprising ZnFe<sub>2</sub>O<sub>4</sub> and ZnO formed on a carbonaceous sacrificial support was reported, as illustrated in **Figure 15**.

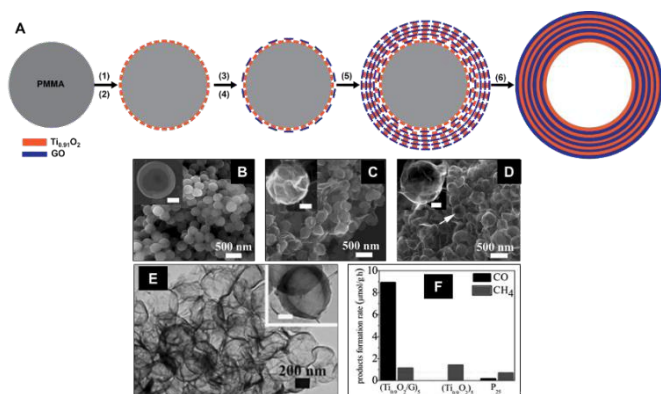


**Figure 16.** A) Schematic illustration of  $\text{TiO}_2/\text{GO}$  hollow composite formation: 1: PEI, 2:  $\text{Ti}_{0.91}\text{O}_2$ , 3: PEI, 4: GO nanosheet, 5: five repeats of steps 1–4, 6: microwave treatment; B,C,D) SEM images of bare PMMA spheres, PEI/ $\text{Ti}_{0.91}\text{O}_2$ /PEI/GO@PMMA, and (G- $\text{Ti}_{0.91}\text{O}_2$ )<sub>5</sub> hollow spheres, respectively; E) TEM image of (G- $\text{Ti}_{0.91}\text{O}_2$ )<sub>5</sub> hollow spheres; F)  $\text{CO}_2$  reduction by (G- $\text{Ti}_{0.91}\text{O}_2$ )<sub>5</sub> hollow spheres.<sup>86</sup>

Simultaneous adsorption of  $\text{Zn}^{2+}$  and  $\text{Fe}^{3+}$  precursors on the negative surface of carbon colloidal spheres causes the formation of the hollow heterojunction structure after calcination. The resulting hollow microstructures are constructed by  $\text{ZnO}$  and  $\text{ZnFe}_2\text{O}_4$  with a size of ca. 15 nm (Figures 15B and 15C). Surprisingly, this nano-sized heterostructure demonstrates remarkable photoactivity for hydrogen evolution without co-catalysts under visible irradiation. This enhancement in photoactivity can be attributed to the homogeneous distribution in the hollow shell of  $\text{ZnO}$  and  $\text{ZnFe}_2\text{O}_4$  as nanoscale particles, which lead to significantly improved charge separation. This work shows that the construction of nanocomposite photocatalysts on the hollow structure can solve the current problems of nanocomposites, i.e., the reduction of charge recombination while exposing a high density of active sites. Moreover, this type of structure could be a lot more convenient for recycling than that of nanocomposite systems alone.<sup>82</sup>

In addition to materials with a semiconductor-semiconductor heterojunction, the development of materials with graphene, which has the unique properties of extra-large surface area, high electron mobility at room temperature, and exceptional thermal conductivity, have been paid considerable attention. The superior mechanical properties and electron transfer ability of graphene helps the composite system prolong charge carrier lifetime and suppresses electron-hole recombination.<sup>83-85</sup> Naturally, hollow structure composites have been produced using this material.

For example, robust hollow spheres constructed from graphene and titania nanosheets have been reported by Tu et al. Titania nanosheets and graphene were sequentially deposited on a PMMA sphere hard template by electrostatic interaction between titania nanosheets (a negatively charged surface), PEI (a polycation), and graphene (a negatively charged surface), as shown in Figure 16. The as-prepared hollow structure promotes  $\text{CO}_2$  photo conversion to  $\text{CH}_4$  which is ten times higher than the commercial product P25. This significant enhancement in photoactivity can be attributed to the high charge separation of the titania nanosheet and graphene heterojunction based on the hollow structure.<sup>86</sup>

Similarly, graphene deposited on  $\text{TiO}_2$  hollow microspheres based on silica or PSS sphere templates has also been reported. Also, hollow heterojunction photocatalysts comprising graphene/ $\text{ZnO}$  and graphene/ $\text{CeO}_2$  have been reported, and show excellent photoactivity in the decomposition of organic pollutants.

The study discussed above indicates that construction of hollow composite structures is becoming an attractive objective that will continue to attract increasing attention from photocatalytic material developers in the future. In addition, employment of hard templates for designing hollow structures is the most appropriate approach to these materials because of the requirement of multiple steps during the fabricating period, an important feature that produces materials capable of improved charge separation. Moreover, the calcination step is probably necessary in order to improve the contact area between individual components.

## Conclusions

Exploitation of sunlight for energy production and environmental remediation is one of the most crucial research topics of the 21st century. Photocatalysis based on semiconductors is an important approach to the utilization of the abundant energy from the sun. Unfortunately, inefficient light absorption and photogenerated charge carrier recombination limits semiconductor-based photocatalyst performance. Thus, development of artificial photosystems that require both efficient sunlight exploitation and charge separation is the most important challenge to be overcome in current photocatalysts.

Utilization of nanoscale photocatalytic systems is a promising approach that can take advantage of the high surface area and high active sites in such materials. Construction of nanoparticle photocatalysts on micro-scale hollow structures exploits the advantages of nano-sized materials in order to reduce charge recombination. In addition, hollow structures possess unique properties that enhance their light absorption ability. For these reasons, the hollow photocatalysts show great promise as candidates for use in efficient artificial photosystems.

Over the last decade, the preparation of hollow photocatalysts has relied mainly on hard template and template-free strategies. In the former, silica spheres, polymer spheres, and carbon colloidal spheres function as the sacrificial support for preparation of the hollow structure. Additionally, the use of metal-organic frameworks as the template has attracted increasing research attention recently. The template-free approach to realising hollow structures is mainly based on physical-chemical phenomena, such as Ostwald ripening, the Kirkendall effect, and ionic exchange.

In this review, we have classified the current study of hollow structure photocatalysts into single-shell, multiple-shell, and composite hollow photosystems, all of which employ a diverse array of semiconductors for different applications. To date, the vast majority of publications are concerned with single-shell materials, due to their simple fabrication

methodology. Moreover, multiple-shell hollow structures with a single semiconductor are rarely reported because of the complexity of their fabrication.

Nanocomposite photocatalysts, the most crucial approach to robust photosystems based on hollow structure materials, still presents many challenges. These challenges are mainly concerned with the development of fabrication strategies and the choice of precursors. Hard templates seem to be the most appropriate sacrificial support because the amount and loading order of the precursors are controllable. Hence, the number and location of individual components in the photocatalytic composite can be precisely dictated.

We believe that photo nanocomposites based on hollow structures offer tremendous promise for the development of future photocatalysts for the following reasons: (i) the formation of large surface area composites, which is impossible by conventional methods; (ii) the high interface area between the individual components, which is an essential factor in suppressing charge recombination; (iii) selective deposition of co-catalysts on the different components in the composite system in order to further boost the photoactivity; (iv) enhancement of light absorption ability.

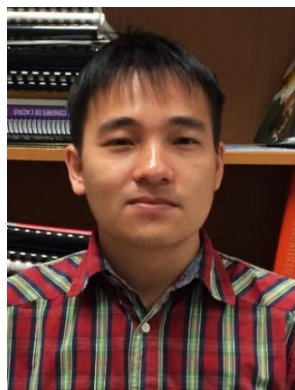
## Acknowledgements

This work was supported by the Natural Science and Engineering Research Council of Canada (NSERC) through the Collaborative Research and Development (CRD) and Discovery grants.

## Notes and references

1. A. Fujishima, *nature*, 1972, **238**, 37-38.
2. C. Chen, W. Ma and J. Zhao, *Chemical Society Reviews*, 2010, **39**, 4206-4219.
3. M. R. Gholipour, C.-T. Dinh, F. Béland and T.-O. Do, *Nanoscale*, 2015, **7**, 8187-8208.
4. H. Tong, S. Ouyang, Y. Bi, N. Umezawa, M. Oshikiri and J. Ye, *Advanced Materials*, 2012, **24**, 229-251.
5. Y. Hou, X. Li, Q. Zhao, X. Quan and G. Chen, *Environmental Science & Technology*, 2010, **44**, 5098-5103.
6. M. Singh, I. Salvadó-Estivill and G. Li Puma, *AIChE Journal*, 2007, **53**, 678-686.
7. H. Wang, L. Zhang, Z. Chen, J. Hu, S. Li, Z. Wang, J. Liu and X. Wang, *Chemical Society Reviews*, 2014, **43**, 5234-5244.
8. K. Wang, Q. Li, B. Liu, B. Cheng, W. Ho and J. Yu, *Applied Catalysis B: Environmental*, 2015, **176-177**, 44-52.
9. J. Li and N. Wu, *Catalysis Science & Technology*, 2015.
10. G. Liu, H. G. Yang, J. Pan, Y. Q. Yang, G. Q. Lu and H.-M. Cheng, *Chemical reviews*, 2014, **114**, 9559-9612.
11. Q. Weng, Y. Ide, X. Wang, X. Wang, C. Zhang, X. Jiang, Y. Xue, P. Dai, K. Komaguchi, Y. Bando and D. Golberg, *Nano Energy*, 2015, **16**, 19-27.
12. Q. Xu, J. Yu, J. Zhang, J. Zhang and G. Liu, *Chemical Communications*, 2015, **51**, 7950-7953.
13. X. Chen, L. Liu, P. Y. Yu and S. S. Mao, *Science*, 2011, **331**, 746-750.
14. L. Yang, H. Zhou, T. Fan and D. Zhang, *Physical Chemistry Chemical Physics*, 2014, **16**, 6810-6826.
15. L. Li, P. A. Salvador and G. S. Rohrer, *Nanoscale*, 2014, **6**, 24-42.
16. R. Marschall, *Advanced Functional Materials*, 2014, **24**, 2421-2440.
17. P. Zhou, J. Yu and M. Jaroniec, *Advanced Materials*, 2014, **26**, 4920-4935.
18. Y. Wang, Q. Wang, X. Zhan, F. Wang, M. Safdar and J. He, *Nanoscale*, 2013, **5**, 8326-8339.
19. J. Low, S. Cao, J. Yu and S. Wageh, *Chemical Communications*, 2014.
20. H. Wang, L. Zhang, Z. Chen, J. Hu, S. Li, Z. Wang, J. Liu and X. Wang, *Chemical Society Reviews*, 2014.
21. M. Dahl, Y. Liu and Y. Yin, *Chemical Reviews*, 2014.
22. R. Jiang, B. Li, C. Fang and J. Wang, *Advanced Materials*, 2014.
23. J. M. Coronado, F. Fresno, M. D. Hernández-Alonso and R. Portela, *Design of advanced photocatalytic materials for energy and environmental applications*, Springer, 2013.
24. Y. Ma, X. Wang, Y. Jia, X. Chen, H. Han and C. Li, *Chemical Reviews*, 2014, **114**, 9987-10043.
25. W.-J. Ong, L.-L. Tan, S.-P. Chai, S.-T. Yong and A. R. Mohamed, *ChemSusChem*, 2014, **7**, 690-719.
26. Y. Lan, Y. Lu and Z. Ren, *Nano Energy*, 2013, **2**, 1031-1045.
27. M. Pelaez, N. T. Nolan, S. C. Pillai, M. K. Seery, P. Falaras, A. G. Kontos, P. S. M. Dunlop, J. W. J. Hamilton, J. A. Byrne, K. O'Shea, M. H. Entezari and D. D. Dionysiou, *Applied Catalysis B: Environmental*, 2012, **125**, 331-349.
28. B. Ma, F. Wen, H. Jiang, J. Yang, P. Ying and C. Li, *Catalysis letters*, 2010, **134**, 78-86.
29. W.-J. Ong, L.-L. Tan, S.-P. Chai and S.-T. Yong, *Dalton Transactions*, 2015, **44**, 1249-1257.
30. J. Ran, J. Zhang, J. Yu, M. Jaroniec and S. Z. Qiao, *Chemical Society Reviews*, 2014, **43**, 7787-7812.
31. S. Bai, L. Wang, X. Chen, J. Du and Y. Xiong, *Nano Res.*, 2015, **8**, 175-183.
32. Q. Xiang, B. Cheng and J. Yu, *Angewandte Chemie International Edition*, 2015, n/a-n/a.
33. W.-J. Ong, L.-L. Tan, S.-P. Chai, S.-T. Yong and A. Mohamed, *Nano Res.*, 2014, **7**, 1528-1547.
34. W.-J. Ong, J.-J. Yeong, L.-L. Tan, B. T. Goh, S.-T. Yong and S.-P. Chai, *RSC Advances*, 2014, **4**, 59676-59685.
35. S. Bai, J. Jiang, Q. Zhang and Y. Xiong, *Chemical Society Reviews*, 2015, **44**, 2893-2939.
36. J. Liu, Y. Liu, N. Liu, Y. Han, X. Zhang, H. Huang, Y. Lifshitz, S.-T. Lee, J. Zhong and Z. Kang, *Science*, 2015, **347**, 970-974.
37. J. Tian, Y. Leng, Z. Zhao, Y. Xia, Y. Sang, P. Hao, J. Zhan, M. Li and H. Liu, *Nano Energy*, 2015, **11**, 419-427.
38. C. Wang and D. Astruc, *Chemical Society Reviews*, 2014, **43**, 7188-7216.
39. F.-H. Du, B. Li, W. Fu, Y.-J. Xiong, K.-X. Wang and J.-S. Chen, *Advanced Materials*, 2014, **26**, 6145-6150.
40. M.-M. Titirici, M. Antonietti and A. Thomas, *Chemistry of Materials*, 2006, **18**, 3808-3812.
41. J. B. Joo, Q. Zhang, I. Lee, M. Dahl, F. Zaera and Y. Yin, *Advanced Functional Materials*, 2012, **22**, 166-174.
42. H. Li, Z. Bian, J. Zhu, D. Zhang, G. Li, Y. Huo, H. Li and Y. Lu, *Journal of the American Chemical Society*, 2007, **129**, 8406-8407.
43. Z. Wang, J. Hou, C. Yang, S. Jiao, K. Huang and H. Zhu, *Energy & Environmental Science*, 2013, **6**, 2134-2144.
44. X. W. Lou, Y. Wang, C. Yuan, J. Y. Lee and L. A. Archer, *Advanced Materials*, 2006, **18**, 2325-2329.
45. H. J. Fan, M. Knez, R. Scholz, D. Hesse, K. Nielsch, M. Zacharias and U. Gösele, *Nano Letters*, 2007, **7**, 993-997.
46. Y. Zhu, D. Fan and W. Shen, *Langmuir*, 2008, **24**, 11131-11136.

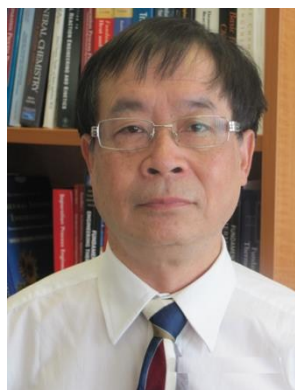
47. J. Sun, J. Zhang, M. Zhang, M. Antonietti, X. Fu and X. Wang, *Nature Communications*, 2012, 1139.
48. R. Gao, S. Zhou, M. Chen and L. Wu, *Journal of Materials Chemistry*, 2011, **21**, 17087-17090.
49. X. Sun and Y. Li, *Angewandte Chemie International Edition*, 2004, **43**, 3827-3831.
50. Y. Li, L. Zhu, Y. Yang, H. Song, Z. Lou, Y. Guo and Z. Ye, *Small*, 2014, n/a-n/a.
51. J. B. Joo, Q. Zhang, I. Lee, M. Dahl, F. Zaera and Y. Yin, *Advanced Functional Materials*, 2012, **22**, 166-174.
52. J. Yu and X. Yu, *Environmental science & technology*, 2008, **42**, 4902-4907.
53. Q. Li, W. Chen, M. Ju, L. Liu and E. Wang, *Journal of Solid State Chemistry*, 2011, **184**, 1373-1380.
54. X.-J. Dai, Y.-S. Luo, W.-D. Zhang and S.-Y. Fu, *Dalton Transactions*, 2010, **39**, 3426-3432.
55. H. Cheng, B. Huang, Y. Liu, Z. Wang, X. Qin, X. Zhang and Y. Dai, *Chemical Communications*, 2012, **48**, 9729-9731.
56. W. Yin, W. Wang and S. Sun, *Catalysis Communications*, 2010, **11**, 647-650.
57. J. Zhang, S. Liu, J. Yu and M. Jaroniec, *Journal of Materials Chemistry*, 2011, **21**, 14655-14662.
58. D. Chen and J. Ye, *Advanced Functional Materials*, 2008, **18**, 1922-1928.
59. J. Huang, R. Ma, Y. Ebina, K. Fukuda, K. Takada and T. Sasaki, *Chemistry of Materials*, 2010, **22**, 2582-2587.
60. Y. Huo, M. Miao, Y. Zhang, J. Zhu and H. Li, *Chemical Communications*, 2011, **47**, 2089-2091.
61. Y. Li, X. Cheng, X. Ruan, H. Song, Z. Lou, Z. Ye and L. Zhu, *Nano Energy*.
62. L. Cao, D. Chen and R. A. Caruso, *Angewandte Chemie*, 2013, **125**, 11192-11197.
63. M. Ibáñez, J. Fan, W. Li, D. Cadavid, R. Nafria, A. Carrete and A. Cabot, *Chemistry of Materials*, 2011, **23**, 3095-3104.
64. J. Qi, K. Zhao, G. Li, Y. Gao, H. Zhao, R. Yu and Z. Tang, *Nanoscale*, 2014, **6**, 4072-4077.
65. S. H. Hwang, J. Yun and J. Jang, *Advanced Functional Materials*, 2014, **24**, 7619-7626.
66. K. E. deKrafft, C. Wang and W. Lin, *Advanced Materials*, 2012, **24**, 2014-2018.
67. J. Lu, P. Zhang, A. Li, F. Su, T. Wang, Y. Liu and J. Gong, *Chemical Communications*, 2013, **49**, 5817-5819.
68. S. Wang, H. Qian, Y. Hu, W. Dai, Y. Zhong, J. Chen and X. Hu, *Dalton Transactions*, 2013, **42**, 1122-1128.
69. C. An, J. Wang, J. Liu, S. Wang and Q.-H. Zhang, *RSC Advances*, 2014, **4**, 2409-2413.
70. P. Xu, R. Yu, H. Ren, L. Zong, J. Chen and X. Xing, *Chemical Science*, 2014, **5**, 4221-4226.
71. J. Chen, D. Wang, J. Qi, G. Li, F. Zheng, S. Li, H. Zhao and Z. Tang, *Small*, 2014.
72. S. Xuan, W. Jiang, X. Gong, Y. Hu and Z. Chen, *The Journal of Physical Chemistry C*, 2008, **113**, 553-558.
73. M. Agrawal, S. Gupta, A. Pich, N. E. Zafeiropoulos and M. Stamm, *Chemistry of Materials*, 2009, **21**, 5343-5348.
74. P. Madhusudan, J. Zhang, B. Cheng and J. Yu, *Physical Chemistry Chemical Physics*, 2015, **17**, 15339-15347.
75. J. Zhang, Z. Zhu, Y. Tang and X. Feng, *Journal of Materials Chemistry A*, 2013, **1**, 3752-3756.
76. M. Wang, J. Han, H. Xiong and R. Guo, *Langmuir*, 2015, **31**, 6220-6228.
77. D. Wang, T. Hisatomi, T. Takata, C. Pan, M. Katayama, J. Kubota and K. Domen, *Angewandte Chemie International Edition*, 2013, **52**, 11252-11256.
78. M.-H. Pham, C.-T. Dinh, G.-T. Vuong, N.-D. Ta and T.-O. Do, *Physical Chemistry Chemical Physics*, 2014, **16**, 5937-5941.
79. H. Ren, R. Yu, J. Wang, Q. Jin, M. Yang, D. Mao, D. Kisailus, H. Zhao and D. Wang, *Nano letters*, 2014, **14**, 6679-6684.
80. C.-T. Dinh, H. Yen, F. Kleitz and T.-O. Do, *Angewandte Chemie International Edition*, 2014, n/a-n/a.
81. Z. Wang, J. Hou, S. Jiao, K. Huang and H. Zhu, *Journal of Materials Chemistry*, 2012, **22**, 21972-21978.
82. H. Song, L. Zhu, Y. Li, Z. Lou, M. Xiao and Z. Ye, *Journal of Materials Chemistry A*, 2015.
83. W.-J. Ong, L.-L. Tan, S.-P. Chai and S.-T. Yong, *Chemical Communications*, 2015, **51**, 858-861.
84. F. Bonaccorso, L. Colombo, G. Yu, M. Stoller, V. Tozzini, A. C. Ferrari, R. S. Ruoff and V. Pellegrini, *Science*, 2015, **347**.
85. W.-J. Ong, L.-L. Tan, S.-P. Chai, S.-T. Yong and A. R. Mohamed, *Nano Energy*, 2015, **13**, 757-770.
86. W. Tu, Y. Zhou, Q. Liu, Z. Tian, J. Gao, X. Chen, H. Zhang, J. Liu and Z. Zou, *Advanced Functional Materials*, 2012, **22**, 1215-1221.



**Chinh-Chien Nguyen** obtained his BSc and MSc degrees in Chemistry Department at Hue University of Sciences- Viet Nam in 2009 and 2011, respectively. He is currently working for his PhD degree at Laval University, Canada under the supervision of Prof. Trong-On Do. His research focuses on the development of sunlight-driven photocatalysts for water splitting and air/water degradation.



**Nhu-Nang Vu** obtained his BSc in Chemistry Department at Ha Noi University of Sciences- Viet Nam in 2014. He is currently working for his PhD degree at Laval University, Canada under the supervision of Prof. Trong-On Do. He focuses on the development of perovskite based photocatalysts for overall water splitting via solar energy.



**Trong-On Do** is a full professor in the Department of Chemical Engineering at Laval University, Canada. He received his MSc in 1986 and PhD in 1989 at University of P. and M. Curie (Paris 6, France). After a period at Brunel University (UK) and the French Catalysis Institute (France), he moved to Laval University in 1990. He then spent two years 1997-1999 in Profs.

Hashimoto/Fujishima's group at Kanagawa Academy of Science and Technology under the Japanese STA Fellowship Award before joining again Laval University as a professor associated with the NSERC Industrial chair. Trong-On Do's research is focused on the design and synthesis of innovative and smart materials and their applications in heterogeneous photocatalysis and renewable energy. He is also a major contributor in the field of zeolite-based materials including controlled-size nanozeolites and hybrid zeolite/mesoporous molecular sieve materials. He has published over 120 papers and review articles in refereed journals and holds 5 international patents. He is the recipient of the 2014 Canadian Catalysis Lectureship Award (CCLA).